Korean J. Chem. Eng., 33(9), 2522-2529 (2016)
DOI: 10.1007/s11814-016-0169-4

pISSN: 0256-1115
eISSN: 1975-7220

Viscosity and rheological properties of ethylene glycol+water+Fe_3O_4 nanofluids at various temperatures: Experimental and thermodynamics modeling

Saeid Atashrouz, Mehrdad Mozaffarian†, and Gholamreza Pazuki

Department of Chemical Engineering, Amirkabir University of Technology (Tehran Polytechnic), Hafez 424, P. O. Box 15875-4413, Tehran, Iran
(*Received 10 December 2015 • accepted 20 June 2016*)

Abstract−The viscosity and rheological behavior of an ethylene glycol-water mixture based Fe_3O_4 nanofluid have been experimentally investigated. The nanofluids for this study were prepared by a two-step method in which Fe_3O_4 nanoparticles were added to a base fluid mixture consisting of 60% (w/w) ethylene glycol and 40% (w/w) water. The measurements were conducted at temperatures ranging from 288.15 to 343.15 K, and at nanoparticle volume fractions ranging from 0.0022 to 0.0055. Furthermore, the dependency of viscosity of nanofluids on shear rate was examined. The results indicate that increasing the shear rate leads to a reduction in the viscosity (shear thinning behavior). Finally, the obtained experimental data was correlated by both a thermodynamic model and a hybrid GMDH-type polynomial neural network, where the mean absolute relative deviation (MARD) of these models was calculated as 3.64% and 3.88%, respectively.

Keywords: Nanofluid, Ethylene Glycol, Fe_3O_4 Nanoparticle, Eyring-MTSM, Carreau-Yasuda

INTRODUCTION

The presence of solid nanoparticles in liquids leads to formation of novel and improved fluids called nanofluids, having the potential to more efficiently perform numerous industrial activities like heat transfer processes [1-3]. The heat transfer properties of nanofluids are more favorable due to the high thermal conductivity (TC) of solid nanoparticles, which can be many times more than that of convectional heat transfer fluids such as ethylene glycol and water. Empirical investigations have revealed that a very low concentration of nanoparticles will result in considerably higher TC. Yang et al. [4] showed that the addition of 0.0035 (v/v) multiwalled carbon nanotubes (MWCNT) to poly (α-olefin) oil helps the fluid TC to rise 200%. This exceptional TC enhancement could mean that aside from the TC effect of nanoparticles, there are other mechanisms involved that can affect the high TC of nanofluids [1]. In this regard, researchers have suggested possible mechanisms, such as the existence of interfacial liquid nanolayer [5-8], Brownian motion effect [9,10], particle clustering effect [11,12], and the effect of increasing the surface area of nanoparticles with decreasing the size of solids [13]. These mechanisms have been successfully explored to interpret the abnormal TC enhancement of the nanofluids. Many of these conducted experiments have been reviewed by Kleinstreuer and Feng [14].

Although numerous studies have been conducted for TC measurement of nanofluids, the rheological behavior and viscosity data of nanofluids have received less attention, bearing in mind that the proper knowledge of the viscosity is of great importance in designing thermal systems, and estimating the required pumping power [15-17]. Murshed et al. [18] reported that the dispersion of 5% Al_2O_3 or TiO_2 nanoparticles (volume fraction) in water will increase viscosity by 82% and 86%, respectively. The elevation of nanofluids' viscosity can bring about serious limitations. As an example, when the viscosity goes up, more pumping energy is needed [19]. Some authors have focused solely on measuring the viscosity of nanofluids; the results of such studies have been extensively reviewed by Mahbubul et al. [20] and Azmi et al. [21].

Most of the earlier experimental researches on nanofluids zeroed in on non-magnetic type of nanofluids rather than on magnetic nanofluids (MNFs). MNFs are a special class of nanofluids that enjoy both magnetic and fluidic properties. Their dual characteristics make it possible to control the flow and heat transfer processes by establishing an external magnetic field [22,23]. Nkurikiyimfura et al. [22] reviewed heat transfer enhancement provided by MNFs. Philip et al. [24] achieved a 300% increment in thermal conductivity of Fe_3O_4-Kerosene MNF with a 0.063 volume fraction of nanoparticles. The augmentation of MNFs TC is primarily due to microstructure changes induced by the external magnetic field on MNFs. When the magnetic field is parallel to the temperature gradient, some particle chains are formed, leading to more effective bridges for energy transport, and consequently boosting the thermal properties of MNFs [22]. Note that despite such dramatic enhancement, employing a magnetic field may not be possible for some industrial applications such as heat exchangers. However, the application of nanofluids based on Fe_3O_4 is not limited to systems affected by a magnetic field. Yu et al. [25] reported 34% enhancement using a Kerosene-based Fe_3O_4 nanofluids with 0.01 volume fraction of nanoparticles. Considering these typical cases, it can be deduced that Fe_3O_4 nanoparticles are an appropriate additive to base fluids for TC enhancement with or without a magnetic field. Sundar et

†To whom correspondence should be addressed.
E-mail: mozaffarian@aut.ac.ir

al. [26] recently published a paper where they claimed a 46% TC enhancement without a magnetic field, merely by addition of 2 vol% of nanoparticle to an ethylene glycol (EG)-water mixture based Fe_3O_4 nanofluid. Nevertheless, they have not reported any viscosity data for the nanofluid. Also, the main reason for considering the EG-water mixture as a base fluid is its applicability in a wide range of temperatures (especially low temperatures).

The objective of this study was to experimentally investigate the viscosity of an EG-water mixture based Fe_3O_4 nanofluid. The effects of volume fraction of nanoparticles, temperature and shear rate on viscosity of the nanofluid were evaluated. Moreover, the Carreau-Yasuda [27] rheological model was coupled with the Eyring-MTSM [28] model so as to form a new model capable of representing the experimental data. In the end, the experimental data was modeled by the group method of data handling (GMDH) system and compared with the proposed model.

NANOFLUID PREPARATION AND VISCOSITY MEASUREMENT

The Fe_3O_4 nanoparticles used in this study were obtained from Sigma Aldrich Company in USA with the properties tabulated in Table 1. A field emission scanning electron microscope (FESEM) image of Fe_3O_4 nanopowder is presented in Fig. 1. As can be seen, the nanoparticle has an approximately cubic shape with a size of 167 nm. Ethylene glycol with purity ≥99% was purchased from Merck Company in Germany, and distilled water was acquired from Zolal Company in Iran.

The base fluid was prepared by mixing a solution of EG and water with a ratio of 60 to 40 (by weight). Then, different amounts of Fe_3O_4 nanopowder were added to the base fluid samples to reach the specified volume fractions of 0.0022, 0.0033, 0.0044, and 0.0055. The volume fraction of nanoparticles was calculated through the following equation:

$$\phi = \frac{\left[\frac{W_{Fe_3O_4}}{\rho_{Fe_3O_4}}\right]}{\left[\frac{W_{Fe_3O_4}}{\rho_{Fe_3O_4}}\right]+\left[\frac{W_{EG}}{\rho_{EG}}\right]+\left[\frac{W_{Water}}{\rho_{Water}}\right]} \quad (1)$$

where ϕ is the volume fraction, ρ is the density, and W is the weight.

The samples were ultrasonicated using a UP200S ultrasonic probe (Hielscher Company, Germany) for 45 min to disperse the nanoparticles in the base fluids. The stability of the nanofluid was quantified in terms of zeta potential, utilizing a Zeta Nano sizer ZS 90 (Malvern Instrument Ltd. UK); the measurements were conducted at 293.15 K. The surface zeta potential graph for a nanofluid containing 0.22 volume concentration of nanoparticles is illustrated in Fig. 2, which clearly indicates that the zeta potential of nanoparticles is −37.7 mV. This value of zeta potential ensures adequate stability of the prepared nanofluid. In addition, the Malvern Nano-Sizer was used for the evaluation of nanoparticle size distribution in the nanofluid, with the results shown in Fig. 3, from which it is apparent that the nanoparticles have a narrow size distribution with an average size of 397 nm. The larger size of nanoparticles in suspension in comparison to dry Fe_3O_4 nano-powder demonstrates that nanoparticles can form aggregates which can influence the viscosity behavior of the nanofluids. Besides, measuring the size of particles by Malvern Nano-Sizer may be regarded as another reason for the larger estimated size of the nanoparticles, since the apparatus gives the hydrodynamic diameter, calculated based on the Stokes-Einstein model, that is expected to be larger than the actual size [29].

Table 1. Physical properties of Fe_3O_4 nanoparticles[a]

Property	Value
Formula weight	231.53 g/mol
Density	4.8-5.1 g/mL at 25 °C
Assay	97% trace metals basis
Surface area	60 m^2/g (BET)

[a]www.sigmaaldrich.com/catalog/product/aldrich/637106

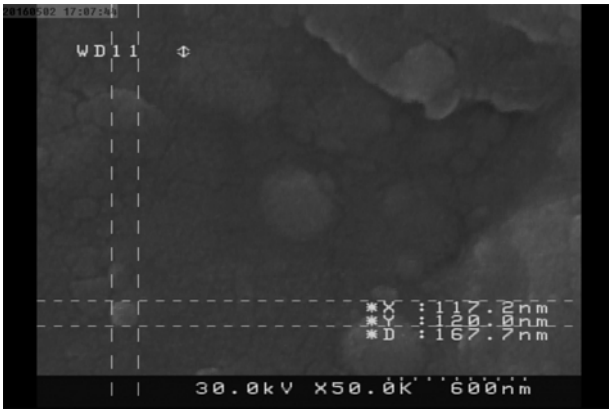

Fig. 1. FESEM image of Fe_3O_4 nanopowder.

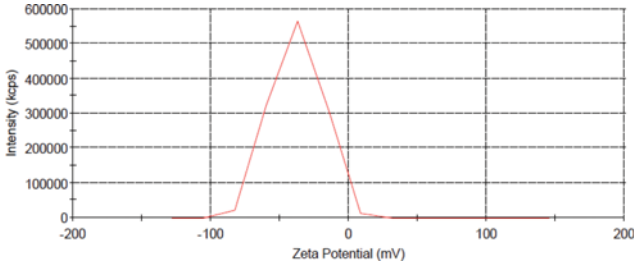

Fig. 2. Surface zeta potential graph for a nanofluid containing 0.22 volume concentration of nanoparticles.

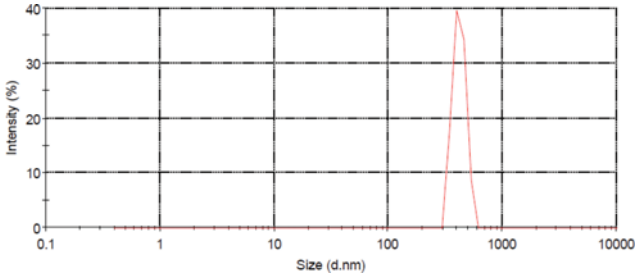

Fig. 3. Size distribution of nanoparticles for a nanofluid containing 0.22 volume concentration of nanoparticles.

The viscosity of nanofluids was measured after ultrasonication by means of a Brookfield viscometer (DV-II+ pro, USA), and the effects of temperature, volume fraction of nanoparticles and shear rate on viscosity were checked. It is worth mentioning that the experimental uncertainty for viscosity measurements in this study was ±0.00015 Pa·s. The uncertainty for temperature regulation was 0.1 °C as well.

MATHEMATICAL MODELING

1. The Eyring-MTSM-Carreau-Yasuda Model

The aim of this section is to construct a model for viscosity estimation of nanofluids as a function of volume fraction of nanoparticles, temperature, and shear rate. The Carreau-Yasuda [27] model is applied in this study to describe viscosity as a function of shear rate:

$$\frac{\eta-\eta_\infty}{\eta_0-\eta_\infty}=[1+(\lambda\dot{\gamma})^a]^{\frac{n-1}{a}} \tag{2}$$

where η is the suspension viscosity, η_∞ is the high shear rate viscosity, and η_0 is the zero shear rate viscosity. λ, a and n are parameters of the Carreau-Yasuda model as well. Obviously, this model has no dependency on the temperature and volume fraction. With the intention of making this model dependent upon the temperature and volume fraction of nanoparticles, an appropriate viscosity model is employed to replace η_0. We recently developed the modified two suffix Margules (MTSM) excess Gibbs free energy model, which was coupled with the Eyring relation for calculation of the viscosity of ionic liquids [28]. In our current study, the Eyring-MTSM model for the nanofluid viscosity estimation can be put into practice as follows:

$$\eta_{mix}=\exp\left(\phi_1\ln(\eta_1)+\phi_2\ln(\eta_2)+\alpha_{12}\frac{\phi_1\phi_2G_{12}G_{21}}{(\phi_1G_{12}+\phi_2)(\phi_2G_{21}+\phi_1)}\right) \tag{3}$$

where subscripts "1" and "2" refer to nanoparticle and base fluid, respectively. Also G_{12} and G_{21} are determined by the following relations:

$$G_{12}=\exp\left(-\frac{\tau_{12}}{RT}\right),\quad \tau_{12}=g_{12}-g_{22} \tag{4}$$

and

$$G_{21}=\exp\left(-\frac{\tau_{21}}{RT}\right),\quad \tau_{21}=g_{21}-g_{11} \tag{5}$$

where g_{ij} is the interaction energy parameter between components i and j.

Thus, with η_0 replaced by η_{mix}, the following becomes the improved Carreau-Yasuda model based on the Eyring-MTSM model:

$$\eta=[1+(\lambda\dot{\gamma})^a]^{\frac{n-1}{a}}\left(\exp\left(\phi_1\ln(\eta_1)+\phi_2\ln(\eta_2)+\alpha_{12}\frac{\phi_1\phi_2G_{12}G_{21}}{(\phi_1G_{12}+\phi_2)(\phi_2G_{21}+\phi_1)}\right)-\eta_\infty\right)+\eta_\infty \tag{6}$$

To incorporate the effect of temperature, α_{12} can be expressed by the following equation:

$$\alpha_{12}=\alpha_{12}^{I}T+\alpha_{12}^{II} \tag{7}$$

Eq. (6) is called Eyring-MTSM-Carreau-Yasuda in the present study (EMCY). The Eyring-NRTL-Carreau-Yasuda model (ENCY) is obtained by the substitution of Eyring-NRTL η_{mix} [30] for η_0 in Eq. (2):

$$\eta=[1+(\lambda\dot{\gamma})^a]^{\frac{n-1}{a}}\left(\exp\left(\phi_1\ln(\eta_1)+\phi_2\ln(\eta_2)+\phi_1\phi_2\left(\frac{A_{21}G_{21}}{\phi_1+\phi_2G_{21}}+\frac{A_{12}G_{12}}{\phi_2+\phi_1G_{12}}\right)\right)-\eta_\infty\right)+\eta_\infty \tag{8}$$

$$A_{ji}=a_{ji}+b_{ji}T \tag{9}$$

and

$$G_{ji}=\exp\left(-\frac{\alpha A_{ji}}{RT}\right) \tag{10}$$

α is a non-random constant parameter, which is set to 0.2 in the present study.

2. Group Method of Data Handling

The application of GMDH [31] has been promoted over the recent years as it delivers both simplicity and accuracy. The group method of data handling was founded on the backbone of natural selection of species. This theory states that the most perfect idiosyncrasies propagate among generations. The GMDH imitates an analogous premise to cross over independent input variables so that a new generation of virtual ones is created. The main advantage of a GMDH system, in comparison to an artificial neural network (ANN), is the mathematical structure of the model. The final mathematical structure of a GMDH model comprises some simple polynomials, while the mathematical structure of an ANN is exceedingly complex [32,33]. After developing the GMDH model, an explicit analytical model representing relevant relationships between input and output variables is derived, whereas ANNs are not able to produce similar simple and explicit relationships.

Therefore, the application of GMDH systems is more convenient, especially in engineering projects. We previously proposed the application of the GMDH method in modeling the viscosity of nanofluids [19]; the experimental viscosity data of nine nanofluid systems were also fed in to optimize the model. That GMDH model was able to successfully estimate the viscosity data with a mean average deviation of 2.14%. We also applied the GMDH approach in other studies to model the surface tension of ionic liquids [34], the activity of polymer solutions [35], and the thermal conductivity of ionic liquids [36]. Hence, having received satisfactory responses from the GMDH model in our former studies, we applied this method to model the experimental viscosity data in the present study.

To initiate the GMDH algorithm, the following matrix is formed as the first step [36]:

$$\begin{matrix} y_1 \\ y_2 \\ \vdots \\ y_N \end{matrix} = \begin{matrix} x_{11} & x_{12} & \cdots & x_{1M} \\ x_{21} & x_{22} & \cdots & x_{2M} \\ \vdots & \vdots & \vdots & \vdots \\ x_{N1} & x_{N2} & \cdots & x_{NM} \end{matrix} \tag{11}$$

where M is the number of independent variables and N is the

number of experimental data. The left hand of the matrix represents the vector of output data ($\vec{V}_y=(y_1, y_2, \ldots, y_N)$), and the right hand represents the vector of independent variables ($\vec{V}_x=(x_1, x_2, \ldots, x_M)$). Then, the algorithm replaces the input variables with the virtual variables (z). Each new virtual variable is defined, involving only two independent variables at a time:

$$z_{ij}=a+b_1x_i+b_2x_j+c_1x_i^2+c_2x_j^2+dx_ix_j \qquad i, j=1, 2, \ldots, M \tag{12}$$

So the matrix of relation (11) is changed as follows:

$$\begin{matrix} y_1 \\ y_2 \\ \vdots \\ y_N \end{matrix} = \begin{matrix} z_{11} & z_{12} & \cdots & z_{1S} \\ z_{21} & z_{22} & \cdots & z_{2S} \\ \vdots & \vdots & \vdots & \vdots \\ z_{N1} & z_{N2} & \cdots & z_{NS} \end{matrix}, \quad S=\begin{pmatrix} M \\ 2 \end{pmatrix} \tag{13}$$

In this set of relations, $S=\begin{pmatrix} M \\ 2 \end{pmatrix}$ is the number of possible combinations of two independent variables taken at a time.

For the purpose of determining the coefficients of the equation, a least square method is adopted. The goal is to minimize the least square (R^2) for each column:

$$R_j^2=\sum_{i=1}^{N_t}(y_i-z_{ij})^2 \qquad j=1, 2, \ldots, S \tag{14}$$

Solving the following equations will generate the coefficients:

$$\frac{\partial(R_j^2)}{\partial a}=-2\sum_{i=1}^{N_t}(y_i-z_{ij})=0 \tag{15}$$

$$\frac{\partial(R_j^2)}{\partial b_1}=-2\sum_{i=1}^{N_t}(y_i-z_{ij})x_i=0 \tag{16}$$

$$\frac{\partial(R_j^2)}{\partial c_1}=-2\sum_{i=1}^{N_t}(y_i-z_{ij})x_i^2=0 \tag{17}$$

$$\frac{\partial(R_j^2)}{\partial d}=-2\sum_{i=1}^{N_t}(y_i-z_{ij})x_{ij}=0 \tag{18}$$

where N_t is the number of data for training the model. It is worth stressing that in the GMDH algorithm just as in the neural networks, some data points are used to train the model and the remaining data points are set aside to test the model. The most accurate polynomial can be found by applying the test data to the generated polynomials in each column of virtual variables. The summation of errors in each column should meet the following criterion:

$$\delta_j^2=\sum_{i=N_t+1}^{N}[y_i-z_{ij}]^2<\varepsilon \qquad j=1, 2, \ldots, S \tag{19}$$

Then, if a virtual variable satisfies the above criterion, it will be saved by the algorithm, otherwise it will be deleted. As the algorithm iterates, it compares the errors and stops when the minimum value is obtained. The topology of the GMDH network consists of intermediate layers in which several nodes combine the interaction of independent and virtual variables to generate nodal expressions from which the explicit expression of the model is gradually derived.

However, the original GMDH approach has disadvantages which undermine its ability to model nonlinear systems. First, it takes only two independent variables at a time to define a virtual variable, and second, it connects the independent variables or virtual variables only to the next layer. Accordingly, in order to model the systems with nonlinear behavior, the mathematical functions of the GMDH should be modified. Hybrid GMDH-type polynomial neural networks (GMDH-PNN) that have been proposed in the literature [19,34-36] allow for the combination of more than two independent variables at a time, and also take account of nodal crossover with different layers. The grand multinomial correlation for a hybrid GMDH-PNN has the following form:

$$y=a+\sum_{i=1}^{M}\sum_{j=1}^{M}\cdots\sum_{k=1}^{M}b_{ij\cdots k}x_i^n x_j^n\cdots x_k^n \qquad n=1, 1, \ldots, 2^l \tag{20}$$

where, stands for number of network layers.

RESULTS AND DISCUSSION

The viscosity of the base fluid was measured, and the results were compared to those in ASHRAE handbook to make sure that the viscometer was accurate (Fig. 4); as it is evident, there is a reasonable conformity between the measured data and those reported

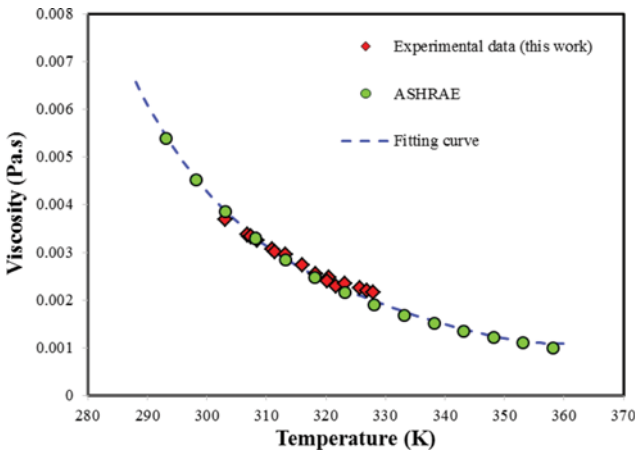

Fig. 4. Comparison of measured viscosity data with ASHRAE handbook data.

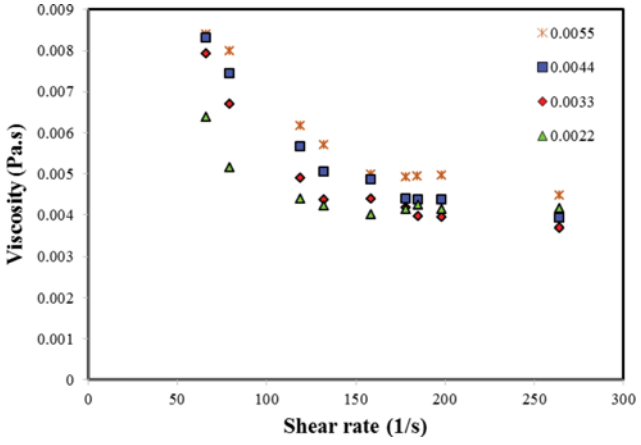

Fig. 5. Viscosity of nanofluids as a function of shear rate at a constant temperature of 303.15 K.

in the ASHRAE handbook. The average absolute relative deviation between ASHRAE data and experimental data in this study is 7.1%. The variation of the nanofluid viscosity with shear rate is presented in Fig. 5 at different volume fractions (and tabulated in Table S1 in supplementary material). The experimental data can support the fact that when the shear rate increases, the viscosity of nanofluids drops sharply. This means that nanofluids exhibit shear thinning behavior like non-Newtonian fluids. This behavior suggests that the Fe_3O_4 nanoparticles will form aggregates in the nanofluid due to attractive forces between particles. These aggregates are broken by applying small forces (shear rates), which in turn lead to a lower viscosity. Moreover, Fig. 5 shows that as shear rate rises, the viscosity of nanofluids reaches a minimum, implying that the Fe_3O_4 nanoparticles have fully dispersed in the base fluid. The effect of temperature on viscosity of nanofluids was investigated by measuring the viscosity of nanofluids, containing different volume fractions of the nanoparticles, at a constant shear rate of 158.4 (1/s), with the results displayed in Fig. 6 (and tabulated in Table S2 in supplementary material). As can be seen, the viscosity of nanofluids declines as the temperature goes up, which confirms the strong dependency of viscosity on temperature.

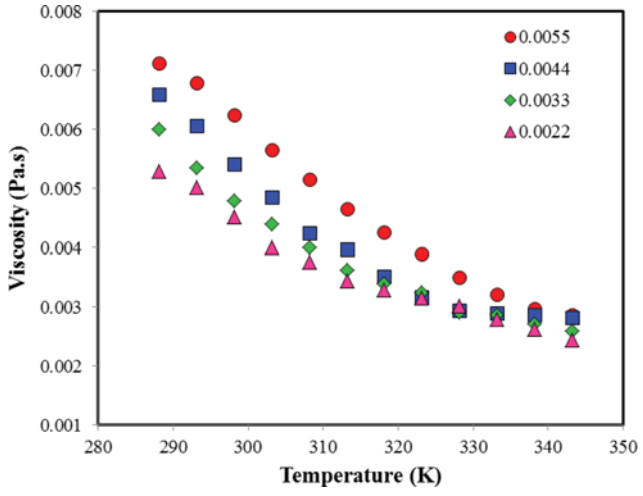

Fig. 6. Experimental viscosity data as a function of temperature at a constant shear rate of 158.41/s.

Fig. 7 demonstrates the shear stress (τ) versus the shear rate ($\dot{\gamma}$) for the nanofluid with a 0.0055 nanoparticle volume fraction. The nanofluid began to flow when the applied shear stress exceeded a certain critical value (yield stress). To model the yield stress in this study, Bingham plastic model, Herschel-Bulkley model, and Casson model were adopted:

$$\text{Bingham plastic model: } \tau = \tau_y + \eta\dot{\gamma} \tag{21}$$

$$\text{Herschel-Bulkley model: } \tau = \tau_y + K_{HB}\dot{\gamma}^n \tag{22}$$

$$\text{Casson model: } \tau^{1/2} = \tau^{1/2} + (\eta\dot{\gamma})^{1/2} \tag{23}$$

where τ_y is the yield stress and η is the suspension viscosity. K_{HB} and n are structure dependent parameters, which can be determined experimentally. The yield stress for each one of the volume fractions was obtained based on the aforementioned models. Fig. 8 shows the yield stress versus the volume fraction of nanoparticles. The yield stress of nanofluid is increased with higher volume fraction of nanoparticles. The Bingham plastic model gave the highest yield stress among the three models, and the estimated results of Herschel-Bulkley model, compared to Casson model, are much closer to those of Bingham plastic model. The lines in Fig. 8 are fitting curves for the models.

The mean average relative deviation (MARD%) is calculated from the following relation:

$$\text{MARD}(\%) = \frac{100}{N}\sum_{i=1}^{N}\left|\frac{\eta^{calc} - \eta^{exp}}{\eta^{exp}}\right| \tag{24}$$

where N is the number of data points, η^{calc} is the calculated viscosity and η^{exp} is the experimental viscosity data.

Table 2 shows the MARD% and parameters of the Carreau-Yasuda model for the experimental data. As mentioned, although this model performs well, there is no contribution of volume fraction of nanoparticles and temperature to the estimated viscosity. Thus, the capability of such models as Eyring-MTSM-Carreau-

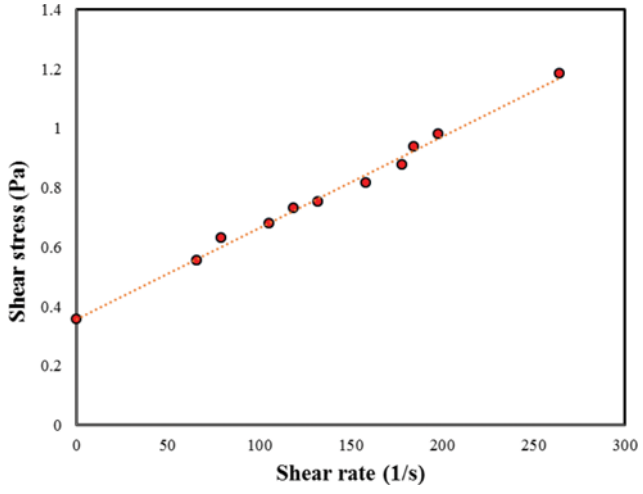

Fig. 7. Shear stress versus shear rate for a 0.0055 volume fraction of nanoparticles.

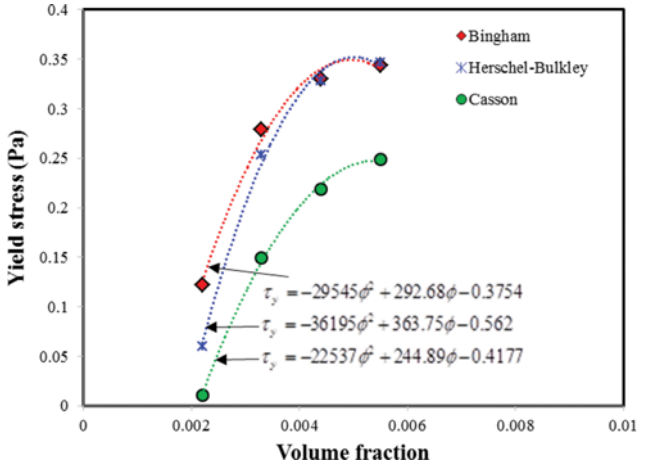

Fig. 8. Yield stress obtained by Bingham plastic, Herschel-Bulkley and Casson models as a function of volume fraction of nanoparticle.

Table 2. MARD% and parameters of Carraeu-Yasuda model at T=303.15 K

ϕ_1	a	n	λ	η_0	η_∞	MARD%
0.0022	0.015106	1028.455	−3.47249	0.00638	0.00415	1.01
0.0033	0.014571	661.2403	−1.31612	0.00792	0.0036	1.66
0.0044	0.013934	626.821	−1.13455	0.0083	0.00382	1.41
0.0055	0.013299	714.2758	−1.07431	0.0084	0.00448	1.85

Table 3. Parameters and MARD% of EMCY and ENCY models

Eyring-MTSM-Carreau-Yasuda							
a	n	λ	α_{12}^{I}	α_{12}^{II}	τ_{21}^{I}	τ_{21}^{II}	MARD%
306.58221	−0.01933	0.02792	−16.01754	6137.93787	1802.97941	14378.46986	3.64
Eyring-NRTL-Carreau-Yasuda							
a	n	λ	a_{12}	b_{12}	a_{21}	b_{21}	MARD%
378.10302	0.01330	0.02475	5794.73315	7.22589	153.79624	−13.92023	4.59

Table 4. Nodal expressions for GMDH model

Input layer
$N_5=0.132541-6.08785\times10^{-5}\dot{\gamma}^2+7783.77\phi_1^3-0.000716891T+1.03501\times10^{-6}T^2$
Intermediate layer 1
$N_4=0.00313957-7.23694\times10^{-19}T^6+91.7801N_5^2$
Intermediate layer 2
$N_3=0.00228213+0.15303\phi1-1.6662N_5+4.5824\times10^{10}N_5^6+824.104N_4^2-86631.6N_4^3$
Intermediate layer 3
$N_2=-1.88019\times10^{-14}+N_3$
Output layer
$\eta=-9.17103\times10^{-15}+0.4719N_3+0.52809N_2$

Yasuda to incorporate the volume fraction of nanoparticles and temperature impacts should be assessed.

To develop the models in this study, 84 experimental data points were used, which are detailed in Tables S1 and S2 (in supporting information). The parameters and MARD% for both the Eyring-MTSM-Carreau-Yasuda (EMCY) and the Eyring-NRTL-Carreau-Yasuda (ENCY) models were obtained based on the experimental data, and are given in Table 3. The EMCY model has a greater accuracy than the ENCY model. Furthermore, to develop the GMDH model, 50% of data points were randomly utilized for training the model, and the other 50% were used for testing the model. The optimized model is detailed in Table 4. The MARD% for all data points is 3.88, indicating that the GMDH model performs better than the ENCY model does. However, the EMCY model has a simpler mathematical form than the GMDH model, and enjoys higher precision for viscosity estimation of nanofluids. Fig. 9 shows the estimated data versus the experimental data for both the EMCY and the GMDH models. The outcomes of the GMDH model in Fig. 9(a) reflect reliably good performance for the trained data as well as broad agreement between the experimental data and the predicted test data. Also, Fig. 10 illustrates the estimated

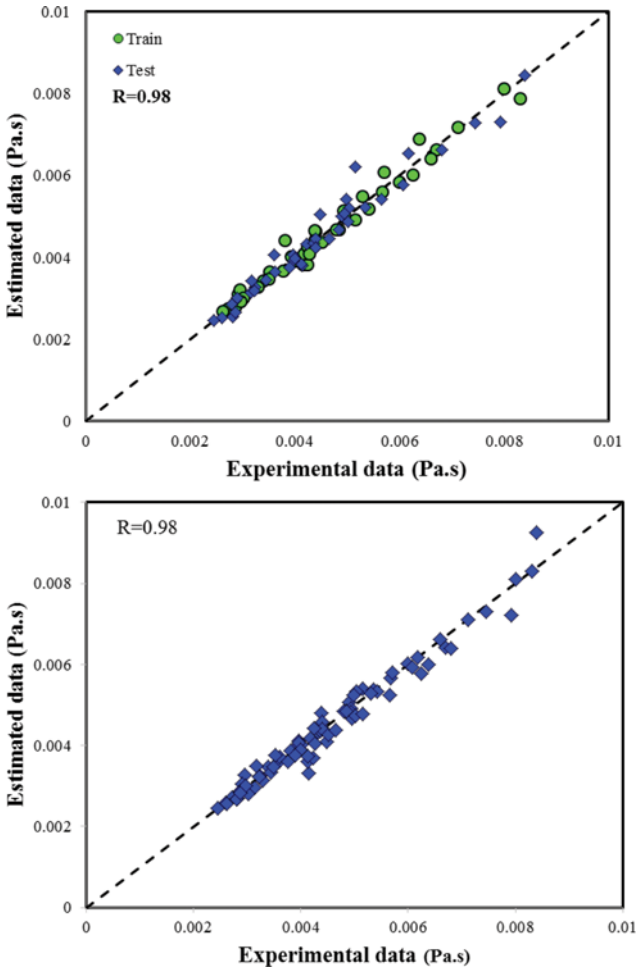

Fig. 9. Estimated data versus experimental data for (a) GMDH model and (b) EMCY model.

viscosity results of the models as a function of temperature, which indicates that both the GMDH and the EMCY models can precisely suggest the trend of nanofluid viscosity.

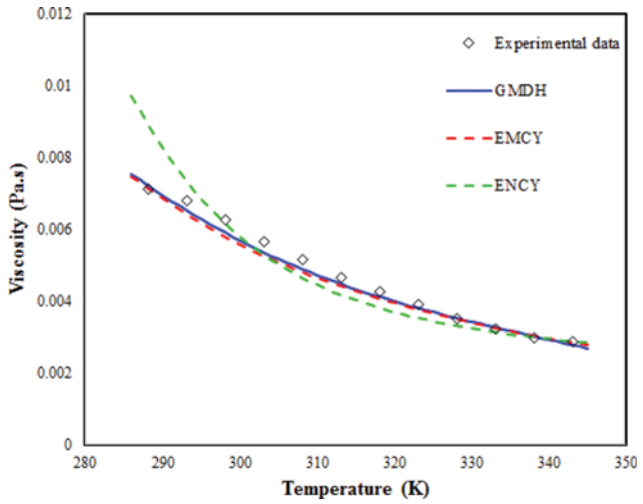

Fig. 10. Comparison of estimated results by the models for $\dot{\gamma}$=158.4 (1/s) and ϕ_1=0.0055.

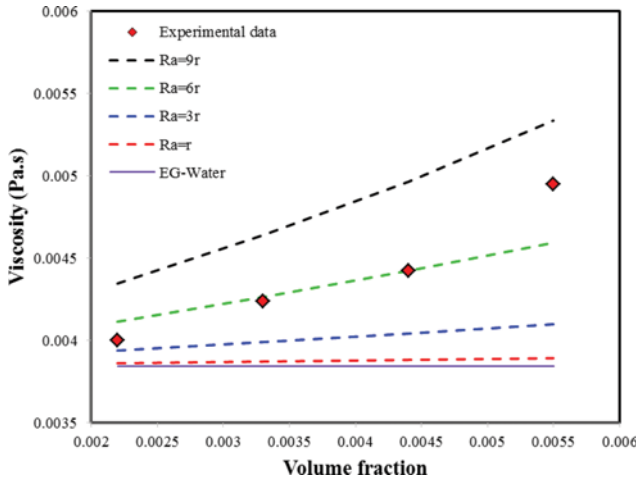

Fig. 11. Predicted results of Eq. (25) for different radius size of aggregates.

As discussed previously, the aggregation of nanoparticles is one of the possible reasons inducing the elevation of the nanofluids viscosity in this study. In an attempt to explore this effect, Chen et al. [37] borrowed the semi-empirical relation of Krieger and Dougherty [38], and proposed the following relation:

$$\frac{\eta(\phi)}{\eta}=\left(1-\frac{\phi}{0.605}\left(\frac{R_a}{r}\right)^{1.2}\right)^{-1.5125} \quad (25)$$

where $\eta(\phi)$ is the suspension viscosity, η_0 is the base fluid viscosity, R_a is the radius of aggregate, and r is the particle radius. Fig. 11 represents the prediction capability of this model at 303.15 K and a shear rate of 158.4 (1/s). The model implies that the suspension viscosity increases for larger radius aggregates. Also, when R_a=6r, the results given by the model are closer to the experimental data. However, these are only approximate values for aggregates' radius which are proposed by Chen et al. [37], and the main reason for making use of such a model is to consider the effect of aggregates on the viscosity of nanofluids. The model also shows that when mono-dispersion of particles occurs, the nanofluid viscosity becomes very close to the base fluid viscosity. In spite of the fact that such low viscosity is very desirable for nanofluids and will lead to low energy consumption, it can diminish the thermal conductivity of nanofluids, since the presence of aggregates in the nanofluids may give rise to the formation of a high conductive path for energy transport [11].

CONCLUSIONS

The viscosity of an ethylene glycol-water mixture based Fe_3O_4 nanofluid was measured at nanoparticle volume fractions ranging from 0.0022 to 0.0055. The Zeta potential of nanofluid was −37.7, which demonstrates sufficient stability of the nanofluid. The study suggests that the formation of aggregates is responsible for increasing the viscosity of nanofluids. The nanofluids behave similar to non-Newtonian fluids, and a shear thinning effect is also observed when shear rates are increased. The semi-empirical models, namely the Bingham plastic model, the Herschel-Bulkley model and the Casson model, were put into use, and all of them indicated a direct relationship between the yield stress and the volume fraction of nanoparticles. Subsequently, EMCY was proposed so as to model the obtained experimental viscosity data. The model has the ability to consider the effects of temperature, volume fraction of nanoparticles and shear rate on the viscosity of nanofluid. The proposed EMCY offers better performance than GMDH and ENCY models, and the MARD% for the three models is 3.64, 3.88 and 4.59, respectively. Nonetheless, the GMDH model is particularly advantageous due to its utilization of 50% of experimental data to test the model, leading to a proper accuracy for both trained and test data.

SUPPORTING INFORMATION

Additional information as noted in the text. This information is available via the Internet at http://www.springer.com/chemistry/journal/11814.

REFERENCES

1. P. Keblinski, S. R. Phillpot, S. U. S. Choi and J. A. Eastman, *Int. J. Heat Mass Transf.*, **45**, 855 (2002).
2. M. Izadi, A. Behzadmehr and M. M. Shahmardan, *Korean J Chem. Eng.*, **31**, 12 (2014).
3. J. Saien and M. Zardoshti, *Korean J Chem. Eng.*, **32**, 2311 (2015).
4. Y. Yang, E. A. Grulke, Z. G. Zhang and G. Wu, *J. Appl. Phys.*, **99**, 114307 (2006).
5. M. E. Meibodi, M. Vafaie-Sefti, A. M. Rashidi, A. Amrollahi, M. Tabasi and H. S. Kalal, *Int. Commun. Heat Mass Transf.*, **37**, 555 (2010).
6. P. Tillman and J. M. Hill, *Int. Commun. Heat Mass Transf.*, **34**, 399 (2007).
7. H. Xie, M. Fujii and X. Zhang, *Int. J. Heat Mass Transf.*, **48**, 2926 (2005).
8. W. Yu and S. U. S. Choi, *J. Nanoparticle Res.*, **5**, 167 (2003).
9. S. P. Jang and S. U. S. Choi, *Appl. Phys. Lett.*, **84**, 4316 (2004).

10. R. Prasher, P. Bhattacharya and P. E. Phelan, *Phys. Rev. Lett.*, **94**, 3 (2005).
11. R. Prasher, P. E. Phelan and P. Bhattacharya, *Nano Lett.*, **6**, 1529 (2006).
12. W. Evans, R. Prasher, J. Fish, P. Meakin, P. Phelan and P. Keblinski, *Int. J. Heat Mass Transf.*, **51**, 1431 (2008).
13. H. Xie, J. Wang, T. Xi, Y. Liu, F. Ai and Q. Wu, *J. Appl. Phys.*, **91**, 4568 (2002).
14. C. Kleinstreuer and Y. Feng, *Nanoscale Res. Lett.*, **6**, 439 (2011).
15. A. S. Dalkilic, A. Çebi, A. Celen, O. Yıldız, O. Acikgoz, C. Jumpholkul, M. Bayrak, K. Surana and S. Wongwises, *Int. Commun. Heat Mass Transf.*, **73**, 33 (2016).
16. M. K. Meybodi, A. Daryasafar, M. M. Koochi, J. Moghadasi, R. B. Meybodi and A. K. Ghahfarokhi, *J. Taiwan Inst. Chem. Eng.*, **58**, 19 (2016).
17. S. Pourfarhang, S. Z. Heris, M. Shokrgozar and M. Kahani, *Korean J. Chem. Eng.*, **32**, 609 (2015).
18. S. M. S. Murshed, K. C. Leong and C. Yang, *Int. J. Therm. Sci.*, **47**, 560 (2008).
19. S. Atashrouz, G. Pazuki and Y. Alimoradi, *Fluid Phase Equilib.*, **372**, 43 (2014).
20. I. M. Mahbubul, R. Saidur and M. A. Amalina, *Int. J. Heat Mass Transf.*, **55**, 874 (2012).
21. W. H. Azmi, K. V. Sharma, R. Mamat, G. Najafi and M. S. Mohamad, *Renew. Sustain. Energy Rev.*, **53**, 1046 (2016).
22. I. Nkurikiyimfura, Y. Wang and Z. Pan, *Renew. Sustain. Energy Rev.*, **21**, 548 (2013).
23. A. Malvandi, *J. Magn. Magn. Mater.*, **406**, 95 (2016).
24. J. Philip, P. D. Shima and B. Raj, *Appl. Phys. Lett.*, **91**, 2005 (2007).
25. W. Yu, H. Xie, L. Chen and Y. Li, *Colloids Surf., A Physicochem. Eng. Asp.*, **355**, 109 (2010).
26. L. S. Sundar, M. K. Singh and A. C. M. Sousa, *Int. Commun. Heat Mass Transf.*, **49**, 17 (2013).
27. R. B. Bird, R. C. Armstrong and O. Hassager, Dynamics of Polymer Liquids, 2nd Ed., Wiley, New York (1987).
28. S. Atashrouz, M. Zarghampour, S. Abdolrahimi, G. Pazuki and B. Nasernejad, *J. Chem. Eng. Data*, **59**, 3691 (2014).
29. L. Zhang, Y. Ding, M. Povey and D. York, *Prog. Nat. Sci.*, **18**, 939 (2008).
30. M. S. Hosseini, A. Mohebbi and S. Ghader, *Chinese J. Chem. Eng.*, **18**, 102 (2010).
31. A. G. Ivakhnenko, *IEEE Trans. Syst. Man. Cybern.*, **1**, 30 (1971).
32. S. Atashrouz and H. Mirshekar, *Bulg. Chem. Commun.*, **46**, 104 (2014).
33. S. Z. Reyhani, H. Ghanadzadeh, L. Puigjaner and F. Recances, *Ind. Eng. Chem. Res.*, **48**, 2129 (2009).
34. S. Atashrouz, E. Amini and G. Pazuki, *Ionics*, **21**, 1595 (2014).
35. S. Atashrouz, G. Pazuki and S. S. Kakhki, *J. Mol. Liq.*, **202**, 95 (2015).
36. S. Atashrouz, M. Mozaffarian and G. Pazuki, *Ind. Eng. Chem. Res.*, **54**, 8600 (2015).
37. H. Chen, Y. Ding and C. Tan, *New J. Phys.*, **9**, 1 (2007).
38. I. M. Krieger and T. J. Dougherty, *J. Rheol.*, **3**, 137 (1959).

Supporting Information

Viscosity and rheological properties of ethylene glycol+water+Fe_3O_4 nanofluids at various temperatures: Experimental and thermodynamics modeling

Saeid Atashrouz, Mehrdad Mozaffarian†, and Gholamreza Pazuki

Department of Chemical Engineering, Amirkabir University of Technology (Tehran Polytechnic), Hafez 424, P. O. Box 15875-4413, Tehran, Iran
(*Received 10 December 2015 • accepted 20 June 2016*)

Table S1. Viscosity data for constant temperature of 303.15 K*

γ	0.22%	0.33%	0.44%	0.55%
66	0.00638	0.00792	0.00830	0.00840
79.2	0.00515	0.00670	0.00745	0.00800
118.8	0.00440	0.00490	0.00567	0.00617
132	0.00423	0.00438	0.00504	0.00570
158.4	0.00400	0.00440	0.00485	0.00498
178.2	0.00413	0.00418	0.00440	0.00493
184.8	0.00424	0.00396	0.00438	0.00495
198	0.00414	0.00394	0.00436	0.00496
264	0.00415	0.00370	0.00392	0.00448

*Uncertainty for viscosity data is Pa·s

Table S2. Viscosity data for constant shear rate of 158.4 (1/s)*

T (Kelvin)	0.22%	0.33%	0.44%	0.55%
288.15	0.00530	0.00600	0.00660	0.00712
293.15	0.00502	0.00535	0.00607	0.00680
298.15	0.00452	0.00480	0.00542	0.00625
303.15	0.00400	0.00440	0.00485	0.00565
308.15	0.00377	0.00401	0.00425	0.00515
313.15	0.00345	0.00362	0.00397	0.00465
318.15	0.00330	0.00340	0.00352	0.00427
323.15	0.00315	0.00325	0.00317	0.00390
328.15	0.00302	0.00292	0.00295	0.00350
333.15	0.00280	0.00287	0.00290	0.00322
338.15	0.00262	0.00272	0.00287	0.00297
343.15	0.00245	0.00260	0.00282	0.00287

*Uncertainty for viscosity data is Pa·s